Carbohydrate Polymers 87 (2012) 289–299

Contents lists available at ScienceDirect

Carbohydrate Polymers

journal homepage: www.elsevier.com/locate/carbpol

Microstructural characterization of chitosan and alginate films by microscopy techniques and texture image analysis

Israel Arzate-Vázquez [a], José Jorge Chanona-Pérez [a,*], Georgina Calderón-Domínguez [a], Eduardo Terres-Rojas [c], Vicente Garibay-Febles [c], Adrián Martínez-Rivas [b], Gustavo Fidel Gutiérrez-López [a]

[a] Departamento de Ingeniería Bioquímica, Escuela Nacional de Ciencias Biológicas, Instituto Politécnico Nacional, Plan de Ayala y Carpio s/n, Col. Santo Tomas, C.P. 11340, Mexico D.F
[b] Centro de Nanociencias y Micro y Nanotecnologías, Instituto Politécnico Nacional, Luis Enrique Erro s/n, Unidad Profesional Adolfo López Mateos, Col. Zacatenco, C.P. 07738, Mexico D.F
[c] Laboratorio de Microscopia de Ultra Alta Resolución, Instituto Mexicano del Petróleo, Eje Central Lázaro Cárdenas 152, Col. San Bartolo Atepehuacan, C.P. 07730. Mexico D.F

ARTICLE INFO

Article history:
Received 3 February 2011
Received in revised form 29 April 2011
Accepted 26 July 2011
Available online 3 August 2011

Keywords:
Chitosan and alginate films
Microscopy techniques
Texture image analysis

ABSTRACT

The aim of this work is to characterize the microstructure of chitosan and alginate edible films by microscopy techniques and texture image analysis. Edible films were obtained by solution casting and solvent evaporation. The microscopy techniques used in this work were: light, environmental scanning electron and atomic force microscopy. Textural features and fractal dimension were extracted from the images. Entropy and fractal dimension were more useful to evaluate the complexity and roughness of films. The highest values of entropy and fractal dimension corresponded to alginate/chitosan, followed of alginate and chitosan films. An entropy/fractal dimension ratio, proposed here, was useful to characterize the degree of image complexity and roughness of edible films at different magnifications. It was possible to postulate that microscopy techniques combined with texture image analysis are efficient tools to quantitatively evaluate the surface morphology of edible films made of chitosan and alginate.

1. Introduction

Biomolecules such as carbohydrates, proteins, lipids or its combinations are used for the preparation of edible coatings and films, which include polysaccharides such as alginates and chitosan (Lin & Zhao, 2007). Alginates are structural biopolymers extracted from brown seaweeds (Sime, 1990) and composed of (1→4)-linked β-D-mannuronate (M) and (1→4)-linked α-L-guluronate (G) units (Ostrowska-Czubenko & Gierszewska-Druzynska, 2009). These units are arranged in G-blocks, M-blocks and alternating sequences of GM-blocks forming the polymeric structure, where the sequential arrangement depends on different factors such as the specie, age or parts of the seaweeds from which this material is obtained (Ashikin, Wong, & Law, 2010; Da Silva, Krause, & Kieckbush, 2009; Rhim, 2004). Due to the good film-forming properties of alginate, different studies relating to the applications of alginate based edible films on fruits and vegetables have been reported (Amanatidou, Slump, Gorris, & Smid, 2000; Lin & Zhao, 2007; Olivas, Mattinson, & Barbosa-Cánovas, 2007; Rojas-Graü, Tapia, Rodríguez, Carmona, & Martín-Belloso, 2007a; Rojas-Graü et al., 2007b; Tay & Perera, 2004; Tapia et al., 2007).

Chitosan is a partially deacetylated polysaccharide that has been widely used in different fields, such as agriculture, horticulture, medicine, water filtration and more. It is produced by the N-deacetylation of chitin, that is a natural polysaccharide found in the exoskeleton of crustaceans and fungal cell walls (Rivero, García, & Pinotti, 2009; Silva et al., 2007). The chemical structure of chitosan is composed of (1→4) linked residues of N-acetyl β-D-glucosamine and (1→4) β-D-glucosamine (Ostrowska-Czubenko & Gierszewska-Druzynska, 2009). The main advantage of chitosan is its strong antimicrobial and antifungal activity to a wide range of microorganisms (Aider, 2010). As in the case of alginate, many studies have reported the use of chitosan as edible coating in foodstuffs (Chien, Sheu, & Yang, 2007a; Chien, Sheu, & Lin, 2007b; Han, Zhao, Leonard, & Traber, 2004; Lin & Zhao, 2007; Park, Stan, Daeschel, & Zhao, 2005; Ribeiro, Vicente, Teixeira, & Miranda, 2007; Vargas, Chiralt, Albors, & González-Martínez, 2009).

As mentioned above, it is possible to produce edible films and coatings by combining different kinds of biomolecules in order to take advantages of each individual component (Rivero et al., 2009). In the case of mixtures made of

* Corresponding author. Tel.: +52 01 57296000x62458; fax: +52 01 5729 62463.
E-mail addresses: alexfe26@yahoo.com.mx (I. Arzate-Vázquez), jorge_chanona@hotmail.com (J.J. Chanona-Pérez), gcalderon@ipn.mx (G. Calderón-Domínguez), eterres@imp.mx (E. Terres-Rojas), vgaribay@imp.mx (V. Garibay-Febles), nanobiomex@hotmail.com (A. Martínez-Rivas), gusfgl@gmail.com (G.F. Gutiérrez-López).

0144-8617/$ – see front matter © 2011 Elsevier Ltd. All rights reserved.
doi:10.1016/j.carbpol.2011.07.044

alginate and chitosan it is well known that these molecules are biocompatible, because electrostatic interactions are formed between carboxyl and amine groups of alginate and chitosan, respectively (Meng et al., 2010; Ostrowska-Czubenko & Gierszewska-Druzynska, 2009).

Nowadays, a plethora of techniques and methods can be used to characterize and evaluate the functionality of edible coatings and films. In the case of edible coatings, it is easier to assess their functionality by measuring qualitative parameters on fruits or vegetables (e.g. weight loss, color, pH and texture) (Lin & Zhao, 2007), but the evaluation of the quality properties of films themselves is a difficult task, as it is necessary to elaborate appropriate samples to be tested, even while the methods to determine physical, thermal, optical, barrier, mechanical and surface properties of these materials have been established perfectly and currently they are applied widely (Rivero et al., 2009; Romero-Bastida et al., 2005; Silva et al., 2007).

Microscopy techniques have also been useful to know the architecture and microstructure of edible films at micro and nanometric scales. Light microscopy (LM), scanning electron microscopy (SEM) and atomic force microscopy (AFM) are techniques more used on the researches of edible films for the characterization of the microstructure and topography (Fahs, Brogly, Bistac, & Schmitt, 2010; Phan, Debeaufort, Luu, & Voilley, 2005; Silva et al., 2007; Veiga-Santos, Suzuki, Nery, Cereda, & Scamparini, 2008; Villalobos, Chanona, Hernández, Gutiérrez, & Chiralt, 2005) while, transmission electron microscopy (TEM) and confocal scanning laser microscopy (CSLM) have been used to characterize ultrastructural and specific observation of some biomolecules in edible films (Andreuccetti, Carvalho, & Grosso, 2009; Denavi et al., 2009). Other important aspect related to the microscopy techniques is the level of magnification used to observe films. The information extracted from the morphology and microstructure of films also depends on the microscopy techniques used. Besides, the effect the magnification has on the estimation of roughness and complexity of films has not been studied, probably because microscopy techniques only provide qualitative information about the microstructure and morphology. However, atomic force microscopy could be considered as an exception since it is possible to obtain quantitative information such as average roughness (R_a) and root mean square roughness (R_q) with this technique (Osés et al., 2009; Villalobos et al., 2005).

The texture image analysis has been suggested in order to measure quantitatively the microstructural changes of foods from images (Quevedo, Mendoza, Aguilera, Chanona, & Gutiérrez-López, 2008). The texture of an image is an attribute representing the spatial arrangement of the gray levels of the pixels, which quantifies some visual characteristics within the image as roughness and smoothness of objects (Du & Sun, 2004; Mendoza, Dejmek, & Aguilera, 2007). Gray Level Co-Ocurrence Matrix (GLCM) and Shifting. Differential Box Counting (SDBC) algorithms have been widely used to estimate textural features and the fractal dimension values, respectively. In the literature, a large number of works using texture image analysis in the food area has been published in recent years (Fernández, Castillero, & Aguilera, 2005; Mendoza et al., 2007; Quevedo et al., 2008; Pérez-Nieto et al., 2010; Quevedo, Jaramillo, Díaz, Pedreschi, & Aguilera, 2010). However, studies of texture image analysis carried out in food materials at microscopic levels are still limited, in particular those ones related to edible films. Therefore, the aim of this work was to characterize the microstructure of edible films made of alginate and chitosan by means of microscopy techniques (LM, ESEM, AFM) and texture image analysis, as a way to test the efficacy of these methodologies as possible tools for the quantitative evaluation of the surface morphology of these materials at different Fields of View (FOV).

2. Materials and methods

2.1. Preparation of edible films

2.1.1. Film-forming solutions

Alginate and chitosan polymers were selected as models to probe the efficacy of image texture analysis for a quantitative evaluation of the microstructure films because these polymers present good compatibility between them and different microstructures as well as they have a well-defined morphology, besides they have been widely used for the preparation of edible films and coatings due to its excellent film-forming properties (Lin & Zhao, 2007).

Thus, sodium alginate (catalog number: 180947) and low molecular weight chitosan (catalog number: 448869) with a deacetylation degree of 75–85% were used to make edible films up. Glycerol (catalog number: G5516) was used as plasticizer to improve the mechanical properties. Solutions of sodium alginate (1%, w/v) were prepared with distilled water at room temperature using a magnetic stirrer (Barnstead International, USA) device for 1 h, and adding while stirring (20 min) glycerol in a ratio of 0.6 g glycerol/1 g polysaccharide. A 1% (w/v) chitosan solution, solubilized in 1% (W/V) acetic acid solution, stirred for 12 h at 80 °C was also prepared. After this time, glycerol was added at the same proportion used for alginate solutions and stirring continued during 20 min. Alginate/chitosan solutions were produced by a mixture of alginate and chitosan solutions at a mass ratio of 1:1 and it was stirred for 30 min. Glycerol and acetic acid were analytical grade. All chemicals were provided by Sigma–Aldrich (St. Louis, USA).

2.1.2. Film formation

Edible films were obtained by solution casting and solvent evaporation technique. Fifteen grams of solution (alginate, chitosan, alginate/chitosan) were poured into glass petri dishes of 60 mm × 15 mm (Pyrex, USA) and dried at 60 °C until reaching constant weight. Once the films were formed, they were removed from the petri dishes and conditioned in a desiccator at 57% (saturated solution of sodium bromide) relative humidity and ambient temperature during 48 h before analysis. In order to corroborate the thickness homogeneity of the films, an electronic micrometer was used (Fowler, IP54, China) with 0.2 μm of accuracy. Measurements were taken at ten different regions on each film sample. The thickness average values of each film were 57.83 ± 1.12 μm (alginate), 57.14 ± 1.5 μm (alginate/chitosan) and 57.51 ± 0.65 μm (chitosan). A one-way Analysis of Variance (one-way ANOVA) and a Tukey multiple comparisons test demonstrated that the thickness of the films had not significant difference ($P > 0.05$).

2.2. Microscopy techniques

2.2.1. Light microscopy (LM)

The surfaces of films were observed by a stereomicroscope (Nikon SMZ 1500, Japan) under transmitted light. Film sections of 2 cm × 2 cm size were placed directly on the microscope base and were observed at three magnifications: 7.5×, 30× and 112.5×; corresponding to Fields of View (FOV) of 28.44 mm^2, 7.36 mm^2 and 0.63 mm^2 respectively. Resolution at each magnification level was 11.11 μm/px, 5.65 μm/px and 1.65 μm/px, respectively. Surface images were captured with a CCD camera (Nikon DS-2Mv, Japan) using the software Nis Elements (F2.30, Nikon, Japan). The acquisition conditions of images were always the same for each magnification in all samples observed (exposure time: 1/1000 s at 7.5×, 1/700 s at 30×, and 1/180 s at 111.25×; gain of 1.0 and contrast in enhanced mode for all magnifications). The images were captured in RGB color and crops of 480 × 480 pixels were stored in TIFF format. For all magnifications, five different areas were taken for each film and three specimens of each film were

evaluated. It is important to highlight that in the Image Analysis (IA) technique several factors must be taken into account, the first and most important are the conditions of image acquisition. The illumination is an essential factor in the acquisition of images and this should be adequate to observe the physical characteristics of interest on the sample (Mendoza, Dejmek, & Aguilera, 2006). In light microscopy, the illumination variables (numerical aperture, diaphragm aperture and light intensity) and the microscope camera settings (exposure time, gain and contrast) were controlled and kept constant for all specimens and magnification levels.

2.2.2. Environmental scanning electron microscopy (ESEM)

The surface microstructure and cross-section of edible films were examined by ESEM (XL 30, Philips, USA). This mode of SEM called environmental mode allows the examination of wet biological specimens without sample preparation (James, 2009), thus films of approximately 5 mm × 5 mm were fixed on the holder using double-sided carbon tape. The films were fractured with liquid nitrogen to observe their cross-section. The samples were observed at 10 kV using the gaseous secondary electron detector. The micrographs were captured in gray-scale and crops of 712 × 418 pixels were stored in TIFF format. These images had a resolution of 0.34 μm/px and a FOV of 0.035 mm^2. Observations of the samples at magnifications of 300× (cross-section) and 500× (surfaces) were performed. For each film magnification, five micrographs were taken; this was done for three specimens of the same type of film. In ESEM, the brightness and contrast are the most important variables that must be controlled during the acquisition of images; therefore, the values of these parameters were kept constant or very similar for all samples at the time of image acquisition. This allows that the texture image analysis and the quantification of the microstructure differences among the samples could be successfully carried out. Other variables such as acceleration voltage and type of electron detector were also considered for the generation of images when applying this technique.

2.2.3. Atomic force microscopy (AFM)

The surface topography of edible films at micro level was analyzed with an AFM (diMultimode V connected to a diNanoscope V microcontroller, Veeco, USA). Small sections of films were scanned with silicon probes (Veeco, USA) with a resonance frequency of 286–362 kHz and spring constant of 20–80 Nm^{-1}. Five areas of film surface (15 μm × 15 μm) were scanned using the tapping mode at 1 Hz of scan rate. The tapping mode was preferred in this work because this method is the most commonly used in the food and biological science fields, therefore it significantly reduces the forces exerted by the tip on the sample as well as the damage that can be exerted on both the sample and the tips, making it suitable for analyzing soft samples such as edible films (Yang et al., 2007). Height (topography) images were obtained, and these images 3D topographic plots of surface films were obtained with the software NanoScope v 7.30 (Veeco, USA). Also, averages values of R_a and R_q (roughness parameters) and section analysis were obtained from height images. All images were collected in RGB color sizing 512 × 512 pixels in TIFF format. These images had a resolution of 0.029 μm/px and FOV of 0.000225 mm^2. All experiments were performed in air at ambient conditions. Three specimens of each film were considered for the experiments. During the quantitative analysis of AFM images it is important to consider two aspects: the image processing operations and the height scale of the image. The image processing operations such as flatten should not be performed because that modify the image information, on the other hand, the height scales of all images must be the same, in order to be able to compare numerical information. These considerations were taken into account in this work.

Table 1
Textural features extracted from grayscale images by GLCM algorithm.

Textural feature	Equation
Energy	$\sum_{ij} P_{d\theta}(i,j)^2$
Contrast	$\sum_{ij} \lvert i-j\rvert^2 P_{d\theta}(i-j)$
Homogeneity	$\sum_{ij} \frac{P_{d\theta}(1-j)}{1+(i-j)}$
Entropy	$-\sum_{ij} P_{d\theta}(i,j)\log(P_{d\theta}(i,j))$

2.3. Texture image analysis

Texture image analysis was applied to quantitatively characterize the surface microstructure of edible films at different FOVs. The image texture is a characteristic representing the spatial arrangement of the gray levels of pixels of the image (Du & Sun, 2004). In this work five textural features were selected as parameters of study (Energy, Contrast, Homogeneity, Entropy and Fractal dimension). All images obtained from microscopy techniques (except ESEM images) were converted from RBG color to gray-scale images; subsequently, Gray Level Co-Ocurrence Matrix (GLCM) and Shifting Differential Box Counting (SDBC) algorithms were applied to obtain textural features from gray-scale images (Haralick, Shanmugam, & Dinstein, 1973; Wen-Shiung, Shang-Yuan, & Chih-Ming, 2003). The whole IA methodology was carried out using the program freeware ImageJ v 1.34s (National Institutes Health, Bethesda, MD, USA).

2.3.1. Gray Level Co-Ocurrence Matrix (GLCM) algorithm

GLCM is a second-order statistic algorithm that compares two neighboring pixels at a time and compiles the frequency at which different gray-levels can be found within a restricted area (Gosselin, Duchesne, & Rodrigue, 2008). Three variables are considered in this algorithm: the number of gray levels (0–255), the distance of the pixels (d) and the angle of displacement (θ) (Haralick et al., 1973). Image texture was analyzed by studying the spatial dependence of pixel values represented by a co-occurrence matrix $P_{d,\theta}$ with entry $P_{d,\theta}$ (i,j) being the relative frequency or distance for two pixels d-pixels apart in direction θ to have values i and j, respectively. According to Haralick et al. (1973), with the GLCM algorithm is possible to calculate fourteen textural parameters. However, we only considered useful: energy, contrast, homogeneity and entropy as the other parameters could be redundant as reported recently (Gosselin et al., 2008; Mendoza et al., 2007). These parameters were measured at a distance d equal to 1 and an angle θ equal to 0°. Table 1 shows the textural parameters extracted from grayscale images with their respective equations.

The energy measures the textural uniformity of the image and is the opposite of entropy. Energy is also known as uniformity, uniformity of energy or angular second moment. The contrast is a measure of local variations of gray level values of images' pixels. Contrast is also known as variance and inertia. Homogeneity, also called inverse difference moment is a measure similar to the energy; which also represents the local homogeneity of the image. Entropy measures the disorder or randomness of images, and can be used to characterize the image texture. It is an indication of the complexity within an image, so the more complex images, the higher entropy values (Haralick et al., 1973; Fernández et al., 2005; Mendoza et al., 2007). These four textural parameters were extracted from gray-scale images acquired by microscopy techniques with the plug-in GLCM Texture included in the software Image J.

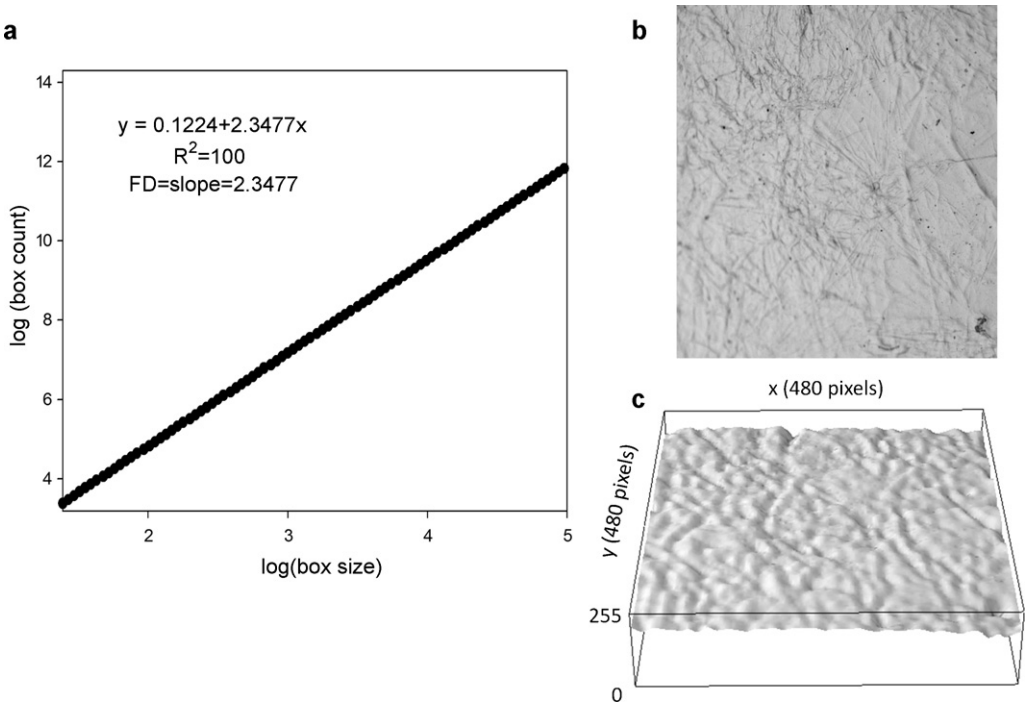

Fig. 1. (a) Plot of log box count versus log box size obtained by using SDBC algorithm, the slope is the fractal dimension of image, (b) LM image in grayscale of alginate/chitosan, (c) Surface intensity plot.

2.3.2. Shifting Differential Box Counting (SDBC) algorithm

Fractal texture was evaluated by power-law scaling to obtain its Fractal Dimension (FD), using Shifting Differential Box Counting (SDBC) method. This algorithm, based on the surface intensity plot (Fig. 1c), is generated from 2-D grayscale images by plotting pixel coordinates (x, y) and its gray level in the z axis (Quevedo et al., 2008; Wen-Shiung et al., 2003). FD was calculated using the ImageJ software by using the SDBC plug-in. FD was estimated from the slope in the log(box count) versus log(box size) plot (Fig. 1a) and by equation 1, where "N" is the number of boxes and "r" is the length of the side box or box size.

$$\mathrm{FD} = \frac{\log(N)}{\log(1/r)} \quad (1)$$

This parameter is a measure directly related to the degree of surface roughness. For 2-D gray-scale images (Fig. 1b) values from 2 to 3 can be obtained, therefore, this value for a rougher surface is higher than that of the smoother one (Quevedo, Jaramillo, Díaz, Pedreschi, & Aguilera, 2009). This parameter was estimated for all grayscale images as obtained for microcopy techniques.

2.3.3. Entropy/fractal dimension ratio

In this work, an entropy/fractal dimension ratio is proposed; this was estimated as the quotient of entropy values divided by fractal dimension values. Entropy/fractal dimension ratio is a composite parameter which associate the complexity of the image in terms of entropy values and image roughness as fractal dimension values. Entropy/fractal dimension ratio value allows the evaluation of the complexity and roughness of an image in a simultaneous way, because frequently a complex image can be associated with a rough one, as in this particulate work, the entropy and fractal dimension values kept a directly proportional relationship. Therefore, the highest values of the entropy/fractal dimension ratio are related to images with a high degree of complexity and roughness, while the lowest values can be associated with simpler and smoother images. Other reports associate the fractal dimension with the complexity of image (Pentland, 1984; Quevedo, Carlos, Aguilera, & Cadoche, 2002). The values of entropy/fractal dimension ratio were used to evaluate the effect of FOV on the complexity and roughness of the films surfaces.

2.4. Statistical analysis

Textural parameters (energy, contrast, homogeneity, entropy, fractal dimension) and roughness parameters (R_a and R_q) were expressed as the mean value with its standard deviation. Statistical comparisons were carried out by one-way Analysis of Variance (one-way ANOVA) followed by a Tukey multiple comparison tests with software Minitab, v. 15. Significant differences were considered when $P < 0.05$. The plots and equations of results were generated using the SigmaPlot software version 10.0.

3. Results and discussion

3.1. Light microscopy (LM)

Fig. 2 shows the LM micrographs of the films at all magnifications, where the alginate and chitosan films showed smoother surfaces at all the magnifications levels, as compared with alginate/chitosan mixture films which presented high roughness. It can be seen from Fig. 2 that the alginate films had a smooth texture with small irregularities homogeneously distributed in the surface. At higher magnification (Fig. 2b and c) it can be observed more details of the irregularities of film surfaces. These irregularities can be associated to the agglomeration of alginate molecules and corresponding to an alginate network formed when the film was dried (Meng et al., 2010; Norajit, Kim & Ryu, 2010). Images with higher roughness and fibrillate structures were observed for the alginate/chitosan films (Fig. 2d–f). The microstructure observed in the alginate/chitosan films could be explained by the electrostatic interactions formed between alginate and chitosan molecules (Ke, Xu, & Yu, 2010). Finally, chitosan films surfaces showed to be very smooth, homogenous and without irregularities (Fig. 2g–i), moreover cracks or holes on the films were not observed. The smoother

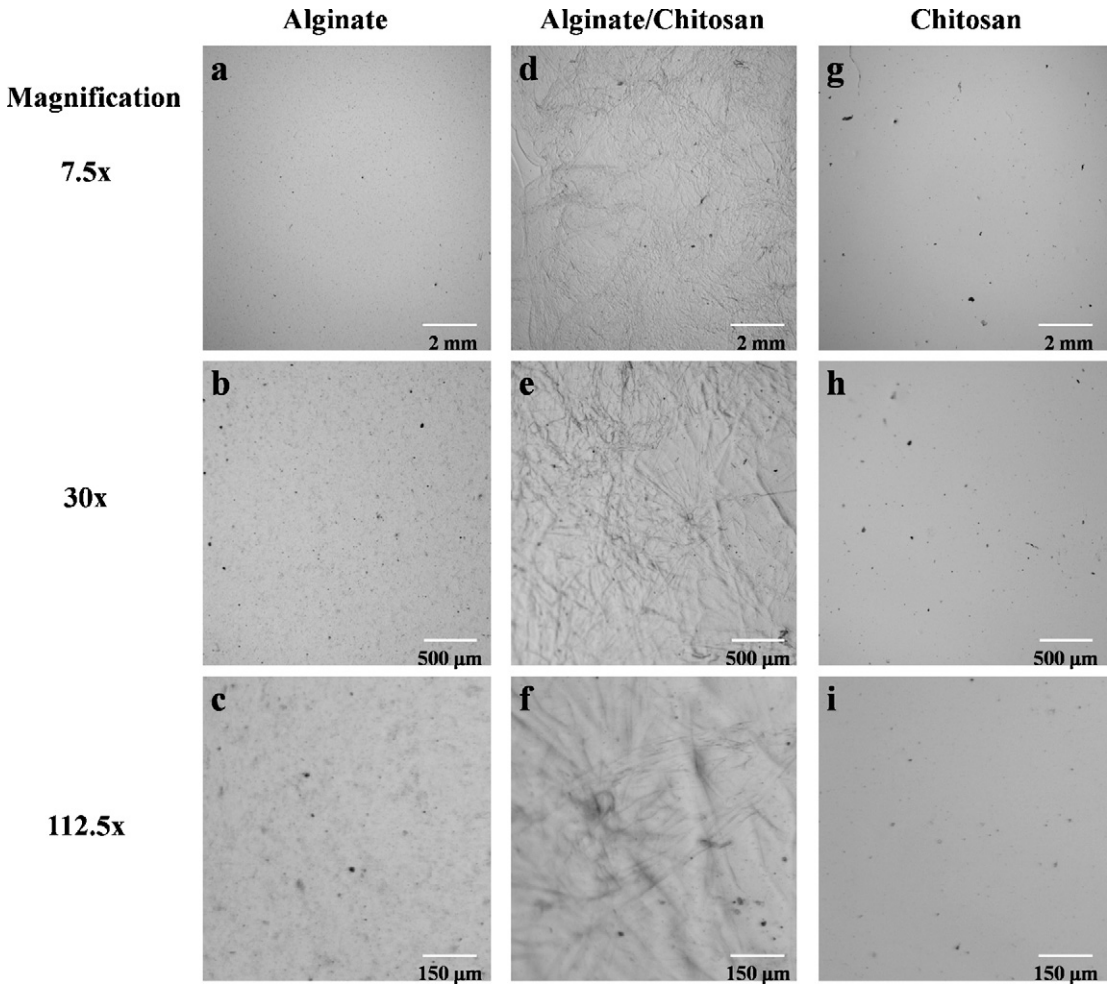

Fig. 2. Selected micrographs of alginate films (a–c), alginate/chitosan films (d–f) and chitosan films (g–i) at different magnifications.

and homogenous surface of chitosan films can be explained by the close packing of chitosan molecules (Meng et al., 2010).

Complementarily to the description of the films microstructure, textural features based on the GLCM and SDBC algorithms were obtained from of LM images and their values are listed in Table 2. As expected, the textural features describe accurately the films texture as observed under LM. For energy values, at the lowest magnification (7.5×), it was not observed significant differences ($P > 0.05$) between the different films. Consequently, as the energy parameter measures the textural uniformity of the image; it is possible to say that at the lowest magnification value, the textural uniformity of the films was similar. In contrast, the values of energy obtained at higher magnification were significantly different ($P < 0.05$); as example, the energy value for chitosan film was $700 \pm 0.00 \times 10^{-5}$, due to it has a uniform texture; while for alginate/chitosan film it was $233 \pm 115.00 \times 10^{-5}$, and with an irregular texture. For the homogeneity parameter, the three types of films evaluated at 7.5× magnification showed significant differences ($P < 0.05$), being this parameter the one that allowed differentiating the films surface textures among samples when they were analyzed at low magnifications (7.5×) as compared with the energy parameter that did not present significant differences between the studied films. In addition, chitosan films had not significant differences ($P > 0.05$) in the homogeneity values at different magnifications, which could be explained as a result of its smooth and homogenous textures in all cases. Alginate/chitosan films had higher values of contrast in comparison with pure films ($P < 0.05$) at 7.5× and 30× magnifications. The highest values of contrast measured on alginate/chitosan films could be due to the fibrillate microstructure forming in the films (Ke et al., 2010). The entropy values of alginate and chitosan films at different magnification did not showed significant differences ($P > 0.05$) among them. The highest values of entropy (8.51 ± 0.04) corresponded to alginate/chitosan films at 7.5× magnification. Finally, the fractal dimension values for all films can be associated with the roughness of the images, as expected, the rougher material (alginate/chitosan mix) showed the largest values of fractal dimension, while the smoother films presented the smallest results. The DF values for each film at different magnification levels did not showed significant differences ($P < 0.05$) with exception of the alginate/chitosan film at 112.5×. However, when the different types of films were compared, at a same magnification level, significant difference was found ($P > 0.05$); with exception of the comparison between alginate and alginate/chitosan films at 112.5×.

Image texture analysis showed to be effective to quantify the microstructure of the surfaces of edible and non edible films as observed by LM; this fact has been reported for other food surfaces in previous works (Briones & Aguilera, 2005; Fernández et al., 2005; Mendoza et al., 2007; Quevedo et al., 2008, 2009). Villalobos et al. (2005) studied the effect that the addition of surfactants on the microstructure and optical parameters of hydroxypropyl methylcellulose films have. By using light microscope, they evaluated the complexity of surface films by using fractal dimension parameter. In other work, Veiga-Santos et al. (2008) studied the efficiency of

Table 2
Textural features extracted from LM images of edible films at different magnifications.

Film type	Magnification/field of view (mm^2)	Textural features				
		Energy ($\times10^{-5}$)	Contrast	Homogeneity ($\times10^{-2}$)	Entropy	Fractal dimension
Alginate	7.5×/59.25	86.00 ± 3.00^{de}	25.04 ± 1.81^{de}	28.56 ± 0.55^{bc}	7.50 ± 0.04^{b}	2.25 ± 0.00^{b}
	30×/15.33	100.00 ± 0.00^{de}	49.53 ± 3.11^{cd}	26.80 ± 0.81^{c}	7.02 ± 0.01^{bc}	2.28 ± 0.02^{b}
	112.5×/1.32	467.00 ± 58.00^{b}	56.62 ± 1.01^{c}	33.03 ± 0.58^{ab}	5.79 ± 0.02^{de}	2.23 ± 0.00^{b}
Alginate/chitosan	7.5×/59.25	30.00 ± 2.00^{e}	111.09 ± 1.99^{a}	13.50 ± 0.72^{e}	8.51 ± 0.04^{a}	2.40 ± 0.01^{a}
	30×/15.33	78.00 ± 15.00^{de}	84.27 ± 10.00^{b}	19.60 ± 0.70^{d}	7.68 ± 0.16^{b}	2.41 ± 0.00^{a}
	112.5× 1.32	233.00 ± 115.00^{c}	56.65 ± 8.28^{c}	30.63 ± 4.35^{bc}	6.55 ± 0.69^{c}	2.27 ± 0.06^{b}
Chitosan	7.5×/59.25	100.00 ± 0.00^{de}	17.97 ± 0.40^{e}	35.86 ± 0.15^{a}	7.11 ± 0.02^{bc}	2.16 ± 0.01^{c}
	30×/15.33	200.00 ± 0.00^{cd}	37.56 ± 3.28^{d}	35.63 ± 0.50^{a}	6.47 ± 0.03^{cd}	2.14 ± 0.01^{c}
	112.5× 1.32	700.00 ± 0.00^{a}	50.76 ± 1.75^{cd}	36.63 ± 0.66^{a}	5.32 ± 0.09^{e}	2.10 ± 0.00^{c}

Values (mean ± standard deviation, $n = 5$) in the same column with the same letters are not significantly different ($P > 0.05$).

light microscopy techniques, as an imaging tool, to evaluate the microstructure of bio-based films. In a recent work, Liu, Qin, He and Song (2009) published results demonstrating the influence of the component ratio that has on the morphologies of starch/chitosan membranes by applying LM, and they could easily observe the phase separation of these components. Therefore, it is possible to say that LM is an essential tool for qualitative studies of edible films surface morphologies, and moreover it has some advantages such as to be an economical and fast tool, that enables the scanning of large sample's areas.

To visualize the effect that the field of view (FOV) and the components ratio have on the textural features, these variables are presented as 3-D plots (Fig. 3). The data were fitted to second order equations (Table 3), with their respective determination coefficients (R^2) and P values for the equation coefficients significance. This correlation analysis was selected for this study because second order equations represent a simple model for visualization of the effect of variables (field of view (FOV) and the components ratio) on the textural features. In addition, adequate determination coefficients (R^2) were obtained for almost all textural features used in this study. The energy and homogeneity parameters had similar tendencies (Fig. 3a and b) and high values of determination coefficients (0.88 and 0.85 respectively) were observed (Table 3), while entropy and fractal dimension showed an opposite pattern (Fig. 3c and d) in

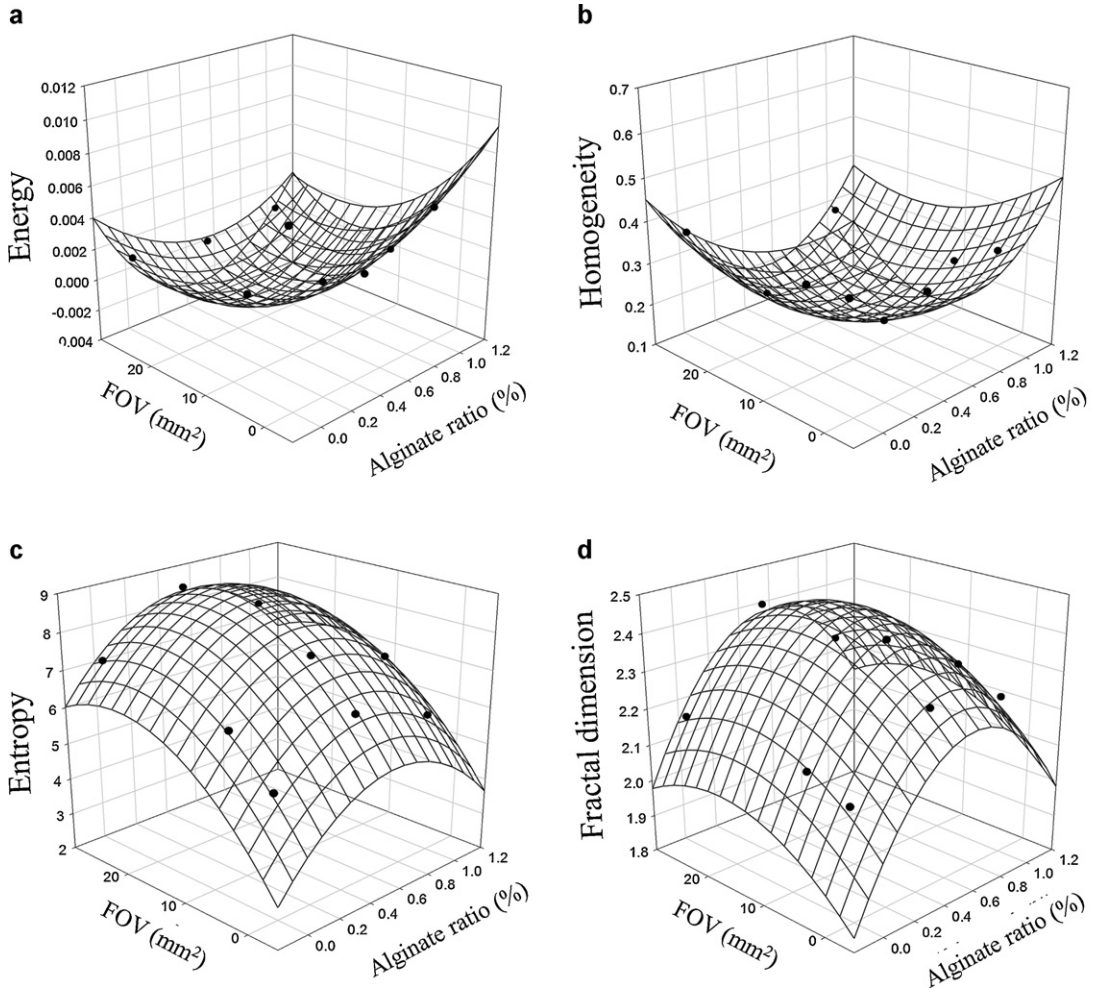

Fig. 3. Textural features as function of FOV and alginate ratio (%): (a) energy, (b) homogeneity, (c) entropy and (d) fractal dimension.

Table 3
Equations, coefficients (R^2) and P values of (z) textural features as function of (x) alginate ratio (%) and (y) FOV (mm^2).

Textural feature	Equation ($z = y_0 + ax + by + cx^2 + dy^2$)	Coefficient (R^2)
Energy	$z = 0.0062–0.0076x - 0.0003y + 0.0065x^2 + 3.98 \times 10^{-6}y^2$	0.88
P values	$y_0 = 0.021$, $a = 0.076$, $b = 0.0219$, $c = 0.1043$, $d = 0.0382$	
Contrast	$z = 35.38 + 186.00x + 0.2624y - 177.70x^2 - 0.0053y^2$	0.62
P values	$y_0 = 0.1544$, $a = 0.0657$, $b = 0.8998$, $c = 0.0667$, $d = 0.8695$	
Homogeneity	$z = 0.4127 - 0.5262x - 0.0055y + 0.4604x^2 - 6.96 \times 10^{-5}y^2$	0.85
P values	$y_0 = 0.0003$, $a = 0.0153$, $b = 0.1833$, $c = 0.0209$, $d = 0.2574$	
Entropy	$z = 5.1699 + 4.6527x + 0.1035y - 4.1791x^2 - 0.0012y^2$	0.99
P values	$y_0 < 0.0001$, $a < 0.0001$, $b = 0.0001$, $c < 0.0001$, $d = 0.0004$	
Fractal dimension	$z = 2.0784 + 0.7904x + 0.0072y - 0.6706x^2 - 9.90 \times 10^{-5}y^2$	0.95
P values	$y_0 = 0.0001$, $a = 0.0013$, $b = 0.0488$, $c = 0.0020$, $d = 0.0671$	

Equation coefficients with P values > 0.05 are not significance.

comparison with energy and homogeneity parameters (Fig. 3a and b). In addition, better R^2 values for entropy (0.99) and fractal dimension (0.95) were obtained. The plot of the contrast parameter was omitted since it presented low R^2 (0.62). P values (Table 3) showed that the FOV was a significant variable for energy parameter while components ratio was significant for homogeneity feature. In the case of entropy and fractal dimension parameters both variables were significant. Contrast parameter showed no dependence with FOV and components ratio.

Fig. 3a shows the effect of FOV as well as the effect of the alginate ratio on the energy parameter. It can be seen from this figure that the energy values increased at low values of FOV, while for all levels of magnification the lowest energy values corresponded to alginate/chitosan films (alginate ratio of 0.5%) and the highest energy values to chitosan film (alginate ratio of 0.0%). A similar tendency was observed for homogeneity parameter (Fig. 3b). These trends can be associated to fibrillate microstructure and heterogeneity of alginate/chitosan films (Ke et al., 2010) that provide surfaces with high levels of heterogeneity (lowest values of energy and homogeneity).

Fig. 3c and d shows the effect of FOV as well as the effect of the alginate ratio on the entropy and the fractal dimension parameters, respectively. Contrary tendencies were observed for the entropy and fractal dimension parameters in comparison with energy and homogeneity. Entropy and fractal dimension parameters were more effective to evaluate the effect of FOV and alginate ratio on complexity and roughness of films surfaces than energy and homogeneity parameters, due to the R^2 coefficients high values obtained. The larger values of entropy can be directly associated with complex images, while the fractal dimension high values with the surfaces roughness (Mendoza et al., 2007; Pérez-Nieto et al., 2010).

3.2. Environmental scanning electron microscopy (ESEM)

Selected ESEM micrographs of surface and cross-section of the films are shown in Fig. 4. The surfaces of alginate films were homogenous, smooth, without pores and with small irregularities as it is shown in Fig. 4a, while the cross-section morphology was compact and also homogeneous and without pores and cracks (Fig. 4b). Norajit et al. (2010) reported that alginate films with glycerol and calcium ions showed a smooth and homogenous surface morphology and also they reported cross-section micrographs with a fibrous-like structure. In addition, a smooth surface morphology for alginate films containing barberine and without glycerol was reported by Ke et al. (2010). In another study Meng et al. (2010) showed that the cross-section morphology of alginate films containing silver sulfadiazine and without glycerol was homogeneous and compact. In the case of alginate/chitosan film surface micrographs, it was possible to observe a fiber network (Fig. 4c) which is

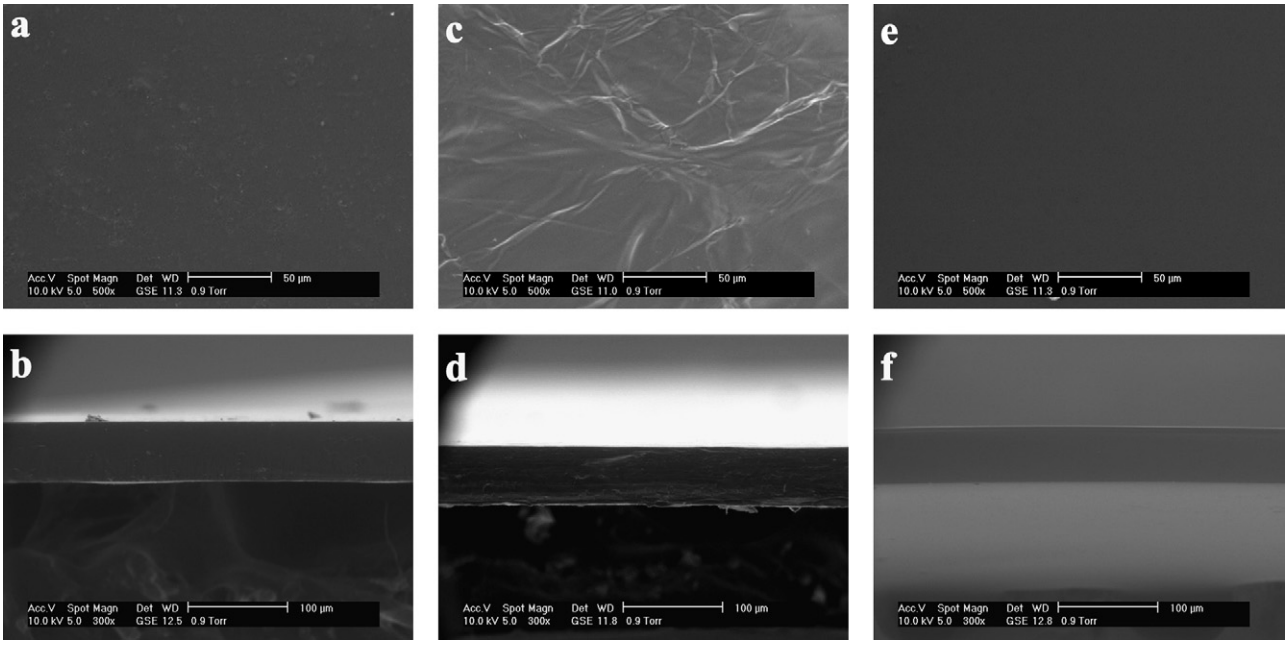

Fig. 4. ESEM micrographs of surface and cross-section of alginate film (a and b), alginate/chitosan film (c and d) and chitosan film (e and f).

Table 4
Textural features extracted from ESEM micrographs of edible films at 500× of magnification.

Film type	Textural features				
	Energy ($\times 10^{-2}$)	Contrast	Homogeneity ($\times 10^{-2}$)	Entropy	Fractal dimension
Alginate	4.20 ± 0.24^{b}	22.23 ± 1.80^{b}	36.22 ± 0.92^{b}	3.50 ± 0.06^{b}	2.14 ± 0.02^{b}
Alginate/chitosan	1.96 ± 0.34^{c}	39.88 ± 5.05^{a}	30.94 ± 1.16^{c}	4.40 ± 0.24^{a}	2.25 ± 0.03^{a}
Chitosan	6.00 ± 0.28^{a}	14.76 ± 1.04^{c}	40.54 ± 0.75^{a}	3.10 ± 0.04^{c}	2.08 ± 0.00^{c}

Values (mean ± standard deviation, $n = 5$) in the same column with the same letters are not significantly different ($P > 0.05$).

typical for films or membranes made with mixtures of both polysaccharides (Ke et al., 2010; Meng et al., 2010). The cross-section morphology of the alginate/chitosan films was less homogeneous than alginate and chitosan films and some pores were observed (Fig. 4d). Finally, we observed more homogeneous, smoother and without pores surfaces and cross-sections on chitosan films in comparison with other films (Fig. 4e and f). Similar descriptions of the morphology of chitosan-based films examined with scanning electron microscopy have been recently reported by others authors (Ke et al., 2010; Meng et al., 2010; Silva et al., 2007).

The scanning electron microscope (SEM) has been throughout the years widely used as a tool for the study and characterizing the microstructure and morphology of edible films. This technique has advantages such as high resolution, fast scanning speed and it is now possible to observe samples in their native state using the environmental mode (ESEM). Nevertheless, one disadvantage of this type of microscope is that the morphological analysis obtained is only qualitative in character, but throughout image analysis quantitative information could be extracted from this ESEM images. In this context and as a way to illustrate the application of texture

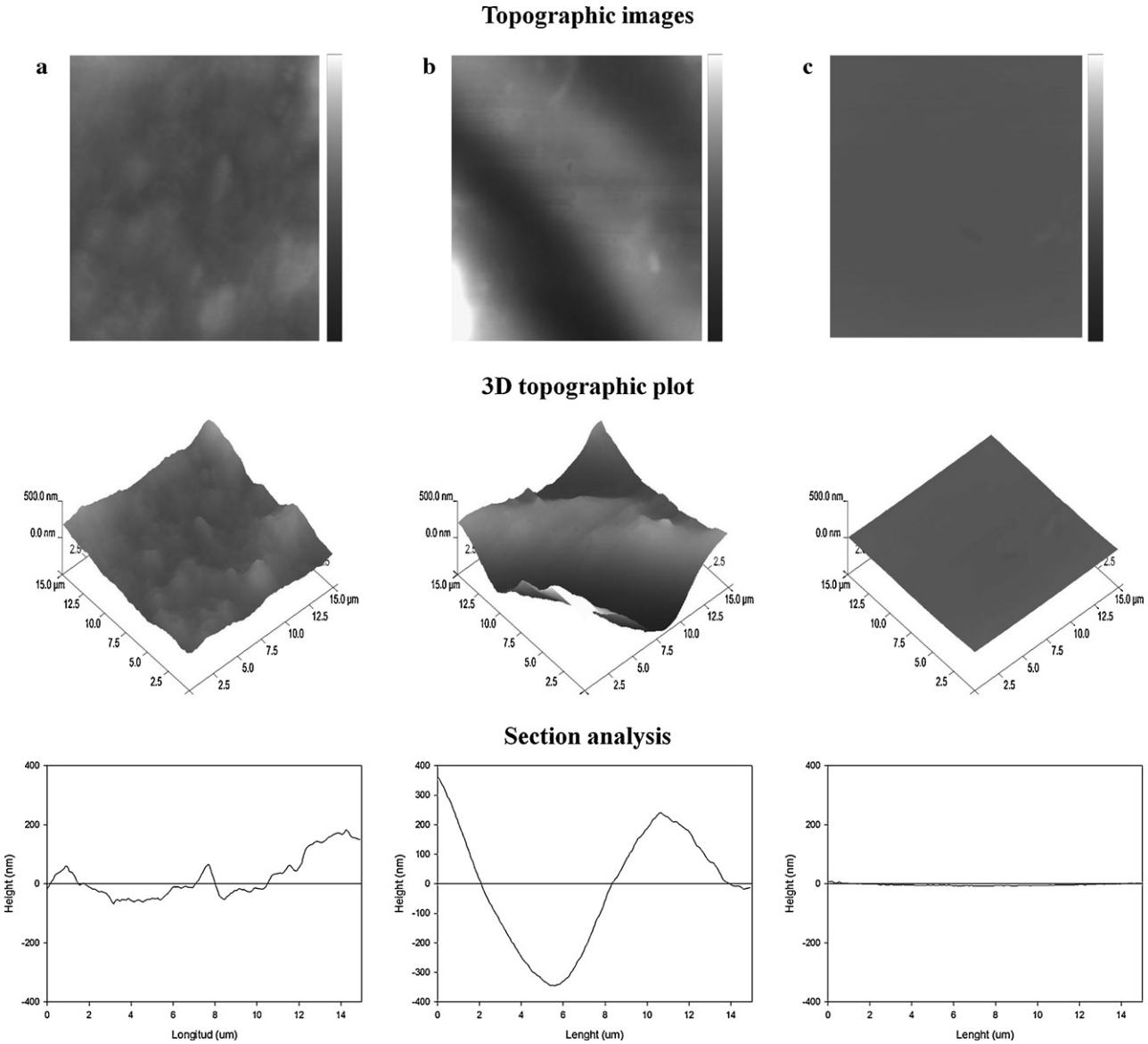

Fig. 5. AFM topographic images (scale bar of 1 μm), below 3D topographic images and section analysis of edible films: (a) alginate, (b) alginate/chitosan and (c) chitosan. Scan size (15 μm × 15 μm).

Table 5
Textural and roughness parameters extracted from AFM topographic images.

Film type	Textural features					Roughness parameters	
	Energy ($\times 10^{-3}$)	Contrast	Homogeneity ($\times 10^{-2}$)	Entropy	Fractal dimension	R_a (nm)	R_q (nm)
Alginate	2.14 ± 0.37^{b}	38.04 ± 11.99^{a}	43.90 ± 1.27^{b}	6.53 ± 0.11^{a}	2.14 ± 0.01^{a}	54.25 ± 14.04^{a}	68.37 ± 16.17^{a}
Alginate/chitosan	3.18 ± 1.94^{b}	32.73 ± 14.77^{a}	47.00 ± 8.80^{b}	6.44 ± 0.52^{a}	2.16 ± 0.04^{a}	53.95 ± 22.20^{a}	69.59 ± 27.21^{a}
Chitosan	86.33 ± 22.36^{a}	26.68 ± 1.32^{a}	84.63 ± 5.34^{a}	3.13 ± 0.42^{b}	2.03 ± 0.04^{b}	8.60 ± 2.06^{b}	11.26 ± 2.56^{b}

Values (mean ± standard deviation, $n = 5$) in the same column with the same letters are not significantly different ($P > 0.05$).

image analysis on ESEM micrographs, a quantitative characterization of the morphology of surface films was developed, selecting only the images obtained with a magnification level of 500×; the values obtained are shown in Table 4. As expected at this level of observation, the textural features allowed quantifying the morphology of the films images obtained by ESEM. The results show there are significant differences ($P < 0.05$) in the mean values of the five textural features for three films (Table 4). For chitosan films, energy and homogeneity parameters showed the highest values ($6.00 \pm 0.28 \times 10^{-2}$ and $40.54 \pm 0.75 \times 10^{-2}$ respectively) in comparison with alginate/chitosan films that showed the lowest values ($1.96 \pm 0.34 \times 10^{-2}$ and $30.94 \pm 1.16 \times 10^{-2}$ respectively). High values of energy parameter were reached when gray level distribution of pixels presented either a constant or a periodic form, while homogeneity feature was associated with local homogeneity of pixels on the image. Low values of energy and homogeneity indicate an irregular distribution and local heterogeneity of pixels on the image respectively (Fernández et al., 2005; Mendoza et al., 2007). These tendencies can be associated with the homogeneous surfaces of chitosan films and heterogonous surfaces of alginate/chitosan films due to the fibers network observed on it. Furthermore, the contrast, entropy and fractal dimension parameters showed inverse trends in comparison with energy and homogeneity, where the chitosan films had the lowest values while the alginate/chitosan films had the highest values (Table 4). In the same context, as the one of light microscopy micrographs, ESEM alginate/chitosan films micrographs had higher values of contrast than the pure films and this can be attributed to the presence of fibers which increase the values of contrast indicating a higher degree of local variations of pixels within the image. Entropy and fractal dimension for the chitosan films were 3.10 ± 0.04 and 2.08 ± 0.00 respectively, in other words this means that the surface texture is more homogenous and smoother than other films. Conversely, the alginate/chitosan films had the highest values of the entropy and fractal dimension and this could be explained by the fiber network resulting in a higher degree of complexity and roughness on the surface. Finally, alginate films showed intermediate values for all textural features in comparison with chitosan and alginate/chitosan films; in this case the low levels of complexity and roughness of alginate films could be explained by an agglomeration phenomenon of alginate molecules (Meng et al., 2010; Norajit et al., 2010).

3.3. Atomic force microscopy (AFM)

AFM topographic images were used as other application example of texture image analysis at low magnification levels. Thus, it is shown in Fig. 5 the AFM topographic images (15 μm × 15 μm, in tapping mode), the 3D topographic plots and the sections analysis of the surface of edible films, where it can be seen that the topography of the alginate films was rough and heterogeneous (3D topographic plots and section analysis). Texture morphology of the alginate/chitosan films is formed by a fibers network (Meng et al., 2010; Norajit et al., 2010) and by means of AFM was possible to examine the topography of these fibers individually as shown in Fig. 5b. As expected the surface topography of chitosan films was extremely smooth and homogenous as shown in Fig. 5c.

The AFM allowed obtaining the roughness parameters such as R_a and R_q and these were calculated for the surfaces of films; these values are listed in Table 5. The alginate and alginate/chitosan films exhibited high values of R_a and R_q, with no-significant differences ($P > 0.05$). The chitosan films presented low values of R_a (8.60 ± 2.06 nm) and R_q (11.26 ± 2.56 nm) in comparison with the other films. Silva et al. (2007) reported a roughness value for chitosan films of 1.8 ± 0.9 nm, which was lower than the one measured in this work, but both results described extremely smooth surfaces.

Textural features extracted from AFM topographic images of the edible films are summarized in Table 5. At this level of FOV, the textural features values of alginate and alginate/chitosan films did not show significant differences ($P > 0.05$). This can be explained considering that images of both films are structurally complex. In contrast, the values of textural features for the chitosan films were significantly different from the other films, with the exception of the contrast parameter, where not differences ($P > 0.05$) were found for three films. Chitosan films showed energy values twenty times larger than the alginate and alginate/chitosan films, due to its high degree of homogeneity. Similar results were found for the homogeneity parameters, where the chitosan film had the highest value as compared with the other films. Entropy values for alginate and alginate/chitosan films were higher than chitosan films; this can be explained by the structural complexity of the surfaces. The fractal dimension of the chitosan films were 2.03 ± 0.04, which is a value close to two, indicating that it is a smoother surface. As expected, there was a relationship between the fractal dimension and roughness parameters, due to the fractal dimension is a parameter that is associated directly with the roughness of an image. Thus, the films (alginate and alginate/chitosan) that showed the highest values of roughness had the highest values of fractal dimension. In the case of chitosan films, they exhibited R_a and R_q lower values than the other films (around five times) and these values correspond to a fractal dimension close to two.

3.4. Entropy/fractal dimension ratio

Entropy/fractal dimension ratio versus FOV's is illustrated in Fig. 6. This figure was divided into three zones corresponding to microscopy techniques used in this work (LM, ESEM and AFM). As can be seen the alginate/chitosan films had the highest values of entropy/fractal dimension ratio with respect to alginate and chitosan films for LM and ESEM; in the case of AFM, alginate films had the highest value (3.04 ± 0.06) as compared with the other films. With regard to LM, it was observed that when decreasing the FOV, the entropy/fractal dimension ratio values diminished gradually. In the case of the three FOV's of LM, the alginate/chitosan films had the highest values, followed by alginate films and last chitosan films. ESEM results showed a similar trend to the one observed in LM images, where the alginate/chitosan films had the high values (1.95 ± 0.07) followed by alginate (1.63 ± 0.02) and last chitosan films (1.49 ± 0.01). In AFM, alginate (3.04 ± 0.06) and alginate/chitosan (2.97 ± 0.24) films showed statistically similar results of the entropy/fractal dimension ratio at the level of FOV used in the experiment, while the chitosan films (1.53 ± 0.17)

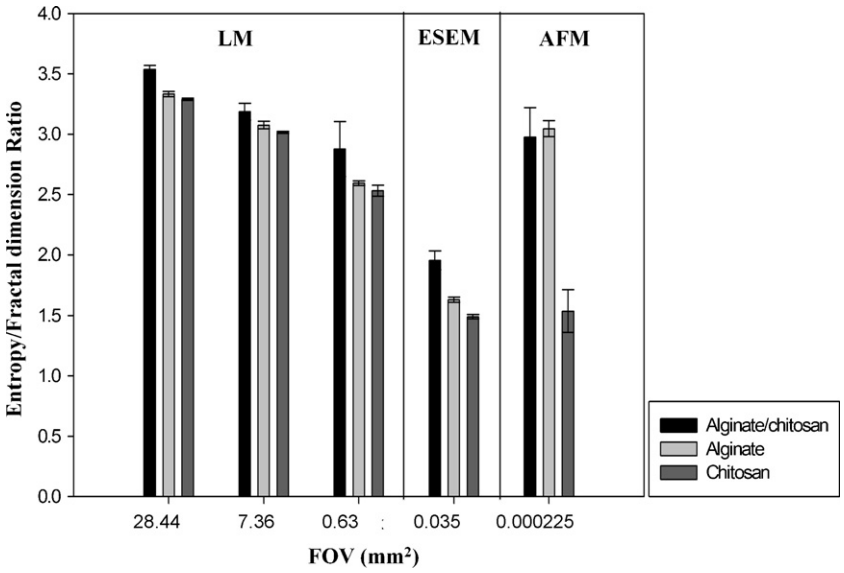

Fig. 6. Values of entropy/fractal dimension ratio of images at different FOV's obtained by LM, ESEM and AFM.

had a lower value due to that they have low complexity and roughness.

An interesting result was found when LM and ESEM were used to study all the films types, where low values of FOV provided low values of entropy/fractal dimension ratio while AFM images supplied higher values for alginate and alginate/chitosan films. When LM and ESEM techniques are used, the changes of magnification promote a reduction in the FOV and as a consequence, the complexity and roughness of the images decrease. When applying AFM, the structural components of alginate and alginate/chitosan films (molecule agglomerates and fibrillate structures) can be observed resulting in high entropy/fractal dimension relation values, while for chitosan films the values were small due to the close packing of chitosan molecules. These results were similar to other reports that mentioned the effect of FOV or magnification relating the values of complexity and roughness of the images. Peleg and Normand (1985) reported that the use of large magnifications can provide low values of roughness (fractal dimension) in coffee agglomerates. Pedreschi, Aguilera, and Brown (2000) referred an inflexion point called smooth-rough crossover for estimation of fractal dimension values, when the images are scanned at different sizes of triangular patches, thus the large sizes of patches provide smooth surfaces. For this reason, ESEM results showed the lowest values of entropy/fractal dimension ratio. These results could be important for the selection of the magnification level and microscopy technique to be used on the study of edible films. Thus, entropy/fractal dimension ratio was successful to characterize the degree of complexity and roughness from surface edible films at different FOV's.

4. Conclusions

On the basis of obtained results it can be concluded that:

(1) For all microscopy techniques used, the films prepared employing the blend of chitosan and alginate resulted in rougher structure while alginate and chitosan films showed smoother structure.
(2) Texture features extracted from LM images were successful to describe quantitatively the microstructure of the studied edible films. The different FOV used in LM technique had an important influence on the values of the textural features. The statistical and correlation analysis allowed differencing the microstructure of edible films studied using this technique.
(3) The texture image analysis results as obtained when analyzing ESEM images of edible films showed significant differences in all the estimated textural parameters.
(4) AFM images resulted in high values of textural features for alginate and alginate/chitosan films in comparison with chitosan films. In addition, FD parameter showed an adequate correlation with roughness parameters (R_a and R_q) as obtained from AFM topographic images.
(5) Entropy and fractal dimension parameters were useful to evaluate the complexity and roughness of films. Therefore, the entropy/fractal dimension ratio was successful for evaluating the complexity and roughness of films. LM and AFM images resulted in similar values for entropy/fractal dimension ratio, with the exception of chitosan film, while ESEM images gives the smallest values as obtained from the microscopic techniques.
(6) The present study showed that texture image analysis is an efficient tool to evaluate quantitatively the microstructure of alginate, chitosan and alginate/chitosan films observed under LM, ESEM and AFM and could be a guide to select the capture conditions and microscopy techniques for the study of edible films.

Acknowledgements

Israel Arzate-Vázquez wishes to thank CONACyT and PIFI-IPN for the scholarship provided. This research was financial through the projects 20100771, 20110627 at the Instituto Politécnico Nacional (IPN-Mexico) and 59730, 133102 from CONACyT. The authors also wish to thank the Centro de Nanociencias y Micro y Nanotecnologías (CNMN) IPN and Instituto Mexicano del Petróleo.

References

Aider, M. (2010). Chitosan application for active bio-based films production and potential in the food industry: Review. *LWT – Food Science and Technology*, doi:10.1016/j.lwt.2010.01.021

Amanatidou, A., Slump, R. A., Gorris, L. G. M., & Smid, E. J. (2000). High oxygen and high carbon dioxide modified atmospheres for shelf life extension of minimally processed carrots. *Journal Food Science*, *65*, 61–66.

Andreuccetti, C., Carvalho, R. A., & Grosso, C. R. F. (2009). Effect of hydrophobic plasticizers on functional properties of gelatin based films. *Food Research International*, *42*, 1113–1121.

Ashikin, W. H. N. S., Wong, T. W., & Law, C. L. (2010). Plasticity of hot air-dried mannuronate- and guluronate-rich alginate films. *Carbohydrate Polymers*, doi:10.1016/j.carbpol.2010.02.002

Briones, V., & Aguilera, J. M. (2005). Image analysis of changes in surface color of chocolate. *Food Research International*, *38*, 87–94.

Chien, P.-J., Sheu, F., & Yang, F.-H. (2007). Effects of edible chitosan coating on quality and shelf life of sliced mango fruit. *Journal of Food Engineering*, *78*, 225–229.

Chien, P.-J., Sheu, F., & Lin, H.-R. (2007). Coating citrus (Murcott tangor) fruit with low molecular weight chitosan increases postharvest quality and shelf life. *Food Chemistry*, *100*, 1160–1164.

Da Silva, M. A., Krause, A. C., & Kieckbush, T. G. (2009). Alginate and pectin composite films crosslinked with Ca^{2+} ions: Effect of the plasticizer concentration. *Carbohydrate Polymers*, *77*, 736–742.

Denavi, G., Tapia-Blácido, D. R., Añón, M. C., Sobral, P. J. A., Mauri, A. N., & Menegalli, F. C. (2009). Effects of drying conditions on some physical properties of soy protein films. *Journal of Food Engineering*, *90*, 341–349.

Du, C.-J., & Sun, D.-W. (2004). Recent developments in the applications of image processing techniques for food quality evaluation. *Trends in Food Science & Technology*, *15*, 230–249.

Fahs, A., Brogly, M., Bistac, S., & Schmitt, M. (2010). Hydroxypropyl methylcellulose (HPMC) formulated films: Relevance to adhesion and friction surface properties. *Carbohydrate Polymers*, *80*, 105–114.

Fernández, L., Castillero, C., & Aguilera, J. M. (2005). An application of image analysis to dehydration of apple discs. *Journal of Food Engineering*, *67*, 185–193.

Gosselin, R., Duchesne, C., & Rodrigue, D. (2008). On the characterization of polymer powders mixing dynamics by texture analysis. *Powder Technology*, *183*, 177–188.

Han, C., Zhao, Y., Leonard, S. W., & Traber, M. G. (2004). Edible coatings to improve storability and enhance nutritional value of fresh and frozen strawberries (*Fragaria ananassa*) and raspberries (*Rubus ideaus*). *Postharvest Biology and Technology*, *33*, 67–78.

Haralick, R. M., Shanmugam, K., & Dinstein, I. (1973). Textural features for image classification. *IEEE Transactions on Systems, Man and Cybernetics SMC*, *3*(6), 610–621.

James, B. (2009). Advances in wet electron microscopy techniques and their application to the study of food structure. *Trends in Food Science & Technology*, *20*, 114–124.

Ke, G., Xu, W., & Yu, W. (2010). Preparation and properties of drug-loaded chitosan–sodium alginate complex membrane. *International Journal of Polymeric Materials*, *59*, 184–191.

Lin, D., & Zhao, Y. (2007). Innovations in the development and application of edible coatings for fresh and minimally processed fruits and vegetables. *Comprehensive Reviews in Food Science and Food Safety*, *6*, 60–75.

Liu, F., Qin, B., He, L., & Song, R. (2009). Novel starch/chitosan blending membrane: Antibacterial, permeable and mechanical properties. *Carbohydrate Polymers*, *78*, 146–150.

Mendoza, F., Dejmek, P., & Aguilera, J. M. (2006). Calibrated color measurements of agricultural foods using image analysis. *Postharvest Biology and Technology*, *41*, 285–295.

Mendoza, F., Dejmek, P., & Aguilera, J. M. (2007). Colour and image texture analysis in classification of commercial potato chips. *Food Research International*, *40*, 1146–1154.

Meng, X., Tian, F., Yang, J., He, C.-N., Xing, N., & Li, F. (2010). Chitosan and alginate polyelectrolyte complex membranes and their properties for wound dressing application. *Journal Material Science: Material Medical*, *21*, 1751–1759.

Norajit, K., Kim, K. M., & Ryu, G. H. (2010). Comparative studies and antioxidant properties of biodegradable alginate films containing ginseng extract. *Journal of Food Engineering*, *98*, 377–384.

Olivas, G. I., Mattinson, D. S., & Barbosa-Cánovas, G. V. (2007). Alginate coatings for preservation of minimally processed Gala apples. *Postharvest Biology and Technology*, *45*, 89–96.

Ostrowska-Czubenko, J., & Gierszewska-Druzynska, M. (2009). Effect of ionic crosslinking on the water state in hydrogel chitosan membranes. *Carbohydrate Polymers*, *77*, 590–598.

Osés, J., Fabregat-Vázquez, M., Pedroza-Islas, R., Tomás, S. A., Cruz-Orea, A., & Maté, J. I. (2009). Development and characterization of composite edible films based on whey protein isolate and mesquite gum. *Journal Food Engineering*, *92*, 56–62.

Park, S., Stan, S. D., Daeschel, M. A., & Zhao, Y. (2005). Antifungal coatings on fresh strawberries (*Fragaria ananassa*) to control mold growth during cold storage. *Journal Food Science*, *70*, M202–M207.

Pedreschi, F., Aguilera, J. M., & Brown, C. A. (2000). Characterization of food surfaces using scale-sensitive fractal analysis. *Journal of Food Process Engineering*, *23*, 127–143.

Peleg, M., & Normand, M. D. (1985). Characterization of the ruggedness of instant coffee particle shape by natural fractals. *Journal of Food Science*, *50*, 829–831.

Pentland, A. (1984). Fractal based description of natural scenes. *IEEE Transactions on Pattern Analysis and Machine Intelligence*, *6*, 661–674.

Pérez-Nieto, A., Chanona-Pérez, J. J., Farrera-Rebollo, R. R., Gutiérrez-López, G. F., Alamilla-Beltrán, L., & Calderón-Domínguez, G. (2010). Image analysis of structural changes in dough during baking. *LWT – Food Science and Technology*, *43*, 535–543.

Phan, D., Debeaufort, F., Luu, D., & Voilley, A. (2005). Functional properties of edible agar-based and starch-based films for food quality preservation. *Journal of Agricultural and Food Chemistry*, *53*, 973–981.

Quevedo, R., Carlos, L. P., Aguilera, J. M., & Cadoche, L. (2002). Description of food surfaces and microstructural changes using fractal image texture analysis. *Journal of Food Engineering*, *53*, 361–371.

Quevedo, R., Mendoza, F., Aguilera, J. M., Chanona, J., & Gutiérrez-López, G. (2008). Determination of senescent spotting in banana (*Musa cavendish*) using fractal texture Fourier image. *Journal of Food Engineering*, *84*, 509–515.

Quevedo, R., Jaramillo, M., Díaz, O., Pedreschi, F., & Aguilera, J. M. (2009). Quantification of enzymatic browning in apple slices appliying the fractal texture Fourier image. *Journal of Food Engineering*, *95*, 285–290.

Quevedo, R., Jaramillo, M., Díasz, O., Pedreschi, F., & Aguilera, J. M. (2010). Quantification of enzymatic browning in apple slices applying the fractal texture Fourier image. *Journal on Food Engineering*, *95*, 285–290.

Rhim, J.-W. (2004). Physical and mechanical properties of water resistant sodium alginate films. *LWT – Food Science and Technology*, *37*, 323–330.

Ribeiro, C., Vicente, A. A., Teixeira, J. A., & Miranda, C. (2007). Optimization of edible coating composition to retard strawberry fruit senescence. *Postharvest Biology and Technology*, *44*, 63–70.

Rivero, S., García, M. A., & Pinotti, A. (2009). Composite and bi-layer films based on gelatin and chitosan. *Journal of Food Engineering*, *90*, 531–539.

Rojas-Graü, M. A., Tapia, M. S., Rodríguez, F. J., Carmona, A. J., & Martín-Belloso, O. (2007). Alginate and gellan based edible coatings as support of antibrowning agents applied on fresh-cut Fuji apple. *Food Hydrocolloids*, *21*, 118–127.

Rojas-Graü, M. A., Raybaudi-Massilia, R. M., Soliva-Fortuny, R. C., Avena-Bustillos, R. J., McHugh, T. H., & Martín-Belloso, O. (2007). Apple puree-alginate edible coating as carrier of antimicrobial agents to prolong shelf-life of fresh-cut apples. *Postharvest Biology and Technology*, *45*, 254–264.

Romero-Bastida, C. A., Bello-Pérez, L. A., García, M. A., Martino, M. N., Solorza-Feria, J., & Zaritzky, N. E. (2005). Physicochemical and microstructural characterization of films prepared by thermal and cold gelatinization from non-conventional sources of starches. *Carbohydrate polymers*, *60*, 235–244.

Silva, S. S., Goodfellow, B. J., Benesch, J., Rocha, J., Mano, J. F., & Reis, R. L. (2007). Morphology and miscibility of chitosan/soy protein blended membranes. *Carbohydrate Polymers*, *70*, 25–31.

Sime, W. J. (1990). Alginates. In P. Harris (Ed.), *Food gels* (pp. 53–58). London: Elsevier Applied Science.

Tapia, M. S., Rojas-Graü, M. A., Rodríguez, F. J., Ramírez, J., Carmona, A., & Martín-Belloso, O. (2007). Alginate- and gellan-based edible films for probiotic coatings on fresh-cut fruits. *Journal of Food Science*, *72*, E190–E196.

Tay, S. L., & Perera, C. O. (2004). Effect of 1-methylcyclopropene treatment and edible coatings on the quality of minimally processed lettuce. *Journal Food Science*, *69*, C131–C135.

Vargas, M., Chiralt, A., Albors, A., & González-Martínez, C. (2009). Effect of chitosan-based edible coatings applied by vacuum impregnation on quality preservation of fresh-cut carrot. *Postharvest Biology and Technology*, *51*, 263–271.

Veiga-Santos, P., Suzuki, C. K., Nery, K. F., Cereda, M. P., & Scamparini, A. R. P. (2008). Evaluation of optical microscopy efficacy in evaluating cassava starch biofilms microstructure. *LWT – Food Science and Technology*, *41*, 1506–1513.

Villalobos, R., Chanona, J., Hernández, P., Gutiérrez, G., & Chiralt, A. (2005). Gloss and transparency of hydroxypropyl methylcellulose films containing surfactants as affected by their microstructure. *Food Hydrocolloids*, *19*, 53–61.

Wen-Shiung, C., Shang-Yuan, Y., & Chih-Ming, H. (2003). Two algorithms to estimate fractal dimension of gray-level images. *Optical Engineering*, *42*(8), 2452–2464.

Yang, H., Wang, Y., Lai, S., An, H., Li, Y., & Chen, F. (2007). Application of atomic force microscopy as a nanotechnology tool in food science. *Journal of Food Science*, *72*(4), R65–R75.